Fuel-Saving Cruising Strategies for Parallel HEVs

Shaobing Xu, Shengbo Eben Li, *Member, IEEE*, Huei Peng, Bo Cheng, Xiaowu Zhang, and Ziheng Pan

***Abstract*—This paper studies the fuel-optimal cruising strategies of parallel hybrid electric vehicles (HEVs) and their underlying mechanisms. To achieve fuel-optimal operations, a discontinuous nonlinear optimal control problem is formulated and solved using the Legendre pseudospectral method and the knotting technique. Three optimal cruising strategies in free/fixed-speed cruising scenarios are proposed: vehicle speed pulse-and-glide strategy, state-of-charge (SoC) pulse-and-glide (PnG) strategy, and constant-speed strategy. The performance and optimal behavior of the engine and the motor are presented, and their fuel-saving mechanisms are explained. Finally, two principles to compromise between fuel economy and ride comfort are proposed and studied.**

***Index Terms*—Eco-driving, hybrid electric vehicle (HEV), optimal control, pseudospectral method, pulse and glide (PnG).**

I. Introduction

TIGHTENING fuel economy standards and environmental concerns continue to pressure the automotive industry into improving the fuel economy of road vehicles [1]–[3]. Technologies such as clean combustion, lightweighting, hybrid powertrains, and intelligent transportation systems have been developed and deployed [4], [5]. Hybrid electric vehicles (HEVs) from Toyota, Ford, Honda, and General Motors have demonstrated significant potential for fuel savings [6], [7]. HEVs are equipped with an energy buffer such as a battery or a supercapacitor [8]–[10]. Hybrid powertrains make it possible to downsize the engine, avoid inefficient engine operation, and execute braking energy recuperation, leading to better fuel economy compared with conventional vehicles [10].

The fuel economy of HEVs depends on a variety of factors, including its powertrain configuration, component sizing, and control strategy [9], [10]. Many optimization-based and rule-based control rules have been developed to improve the fuel economy of HEVs in diverse driving scenarios and cycles [11]–[13]. In this paper, we focus on designing fuel-optimal control strategies in cruising scenarios for parallel HEVs. Parallel hybrid powertrains are used in Honda, Hyundai, and many European hybrid vehicle models [14], [15]. Cruising consumes a significant portion of the total energy, that is, 35% under urban conditions [16] and even higher on the highways. Research has shown that coach buses spend 65%–78% of their total driving time cruising on the freeways in Beijing [17]. It was estimated that a 1% fuel savings in cruising scenarios can save 20 million barrels of oil per year worldwide [18].

In cruising scenarios, constant-speed (CS) operation is frequently used. For conventional vehicles, this means operating the engine and transmission at a constant state. Instead of the CS strategy, vehicles can cruise in a pulse-and-glide (PnG) fashion, which is a strategy commonly used in super-mileage competition vehicles [19], [20]. The PnG strategy has been proven to achieve better fuel economy than the CS operation, with up to 20% fuel savings [20]–[22]. Lee *et al.* validated the fuel-saving performance in experiments [19]. For nonhybrid vehicles with a continuously variable transmission (CVT), Li and Peng provided analytical results of how the PnG strategy works [20], [21]. In this case, the vehicle inertia acts as a kinetic "energy buffer." It allows the engine to operate efficiently and intermittently, resulting in a higher average efficiency than the CS operation [20]. Despite the better fuel economy, the fluctuating speed of the PnG strategy leads to deteriorated ride comfort [19]–[21].

Parallel HEVs contain both electric energy buffer (i.e., battery) and mechanical "energy buffer" (i.e., vehicle inertia). The additional energy buffer expands the freedom in power management. Instead of "swinging the vehicle speed high and low," the battery state of charge (SOC) can be fluctuated as an alternative to improve ride quality. In fact, both vehicle kinetic energy and battery energy can be rocked back and forth for optimal fuel economy or better tradeoff between fuel economy and ride comfort.

The main contribution of this paper is to systematically study how the dual-energy-storage system can be used for optimal fuel economy and its tradeoff against ride comfort. More specifically, 1) we first study the fuel-optimal cruising strategy for parallel HEVs, including the coordination between mechanical energy buffer and the battery energy buffer. 2) The underlying fuel-saving mechanism is then explained. 3) Two simple rules to compromise between fuel economy and ride comfort are then proposed. The rest of this paper is organized as follows: Section II describes the model of a parallel HEV and the fuel-optimal cruising problem, Section III presents the method for solving the problem, Section IV presents the optimal cruising operations under different speed constraints, Section V analyzes the fuel-saving mechanisms of the optimal operations, and Section VI presents the rules to compromise between fuel economy and ride comfort. Finally, Section VII concludes this paper.

Manuscript received March 16, 2015; revised July 22, 2015; accepted October 7, 2015. Date of publication October 12, 2015; date of current version June 16, 2016. This work was supported in part by the National Natural Science Foundation of China under Grant 51205228 and 51575293, and in part by the Tsinghua University Initiative Scientific Research Program under Grant 2012THZ0. The first two authors, i.e., S. Xu and S. E. Li, contributed equally to this work. The review of this paper was coordinated by Prof. M. Benbouzid. *(Corresponding author: Shengbo Eben Li.)*

S. Xu, S. E. Li, and B. Cheng are with the State Key Laboratory of Automotive Safety and Energy, Department of Automotive Engineering, Tsinghua University, Beijing 100084, China (e-mail: xsbing2008@foxmail.com; lisb04@gmail.com; chengbo@tsinghua.edu.cn).

H. Peng is with the Department of Mechanical Engineering, University of Michigan, Ann Arbor, MI 48109 USA, and also with the State Key Laboratory of Automotive Safety and Energy, Tsinghua University, Beijing 100084, China (e-mail: hpeng@umich.edu).

X. Zhang and Z. Pan are with the Department of Mechanical Engineering, University of Michigan, Ann Arbor, MI 48109 USA (e-mail: xiaowuz@umich.edu; zihpan@umich.edu).

Color versions of one or more of the figures in this paper are available online at http://ieeexplore.ieee.org.

Digital Object Identifier 10.1109/TVT.2015.2490101

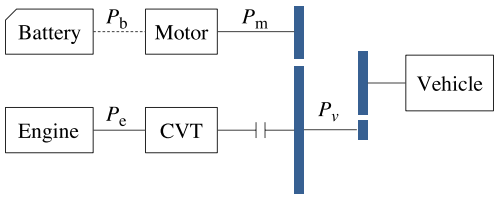

Fig. 1. Powertrain topology of the parallel HEV.

II. Hybrid Electric Vehicle Model and Problem Statement

The studied parallel HEV involves a mechanical and an electric powertrain, with its topology shown in Fig. 1. The main components are the internal combustion engine, CVT, clutch, battery, motor, torque coupler, and vehicle. The power generated by the engine can be used to drive the vehicle and/or to charge the battery. The engine and the motor can drive the vehicle individually or together. This section describes the models of these components.

Since our goal is to obtain the control rules for the engine and motor to minimize fuel consumption, the problem naturally fits into an optimal control framework, with engine power and motor power as control inputs. The performance index, plant dynamics, and constraints of this fuel optimal control problem (OCP) are described as follows.

For simplicity, the following assumptions are made.

1) The dynamics of the fly-wheel, clutch, CVT, and motor are ignored.
2) The engine always operates on the best brake-specific fuel-consumption (BSFC) line by using the CVT.

A. Performance Index for Fuel Economy

The index "fuel consumption per 100 kilometers" is used to measure the fuel economy, which is defined as

$$J = \frac{\int_0^{t_f} \mathcal{F}_e dt}{s_f} \tag{1}$$

where t_f, $\mathcal{F}_e$, and s_f denote the terminal time, the engine fuel injection rate, and the terminal distance, respectively.

The engine BSFC map is shown in Fig. 2(a), where the point with maximum efficiency is called the sweet spot (power: 18.9 kW; efficiency: 38.3%).

The best BSFC line, which is the collection of the most efficient points for varying power levels, is shown in Fig. 2(a). Its efficiency η_e is fitted by

$$\eta_e = \eta_0 + \sum_{i=1}^{3} k_i (P_e - P_0)^{\frac{1}{2i}} \tag{2}$$

where η_0 and k_i are the fitting coefficients, P_e is the engine power, and P_0 is a constant. The fitting result is shown in Fig. 2(b). Since the engine always operates on the best BSFC line, the engine fuel injection $\mathcal{F}_e$ rate is obtained by

$$\mathcal{F}_e = \frac{P_e}{c_g \times \eta_e(P_e)} \tag{3}$$

where c_g is the calorific value of gasoline. If the engine is shut off, then $\mathcal{F}_e = 0$.

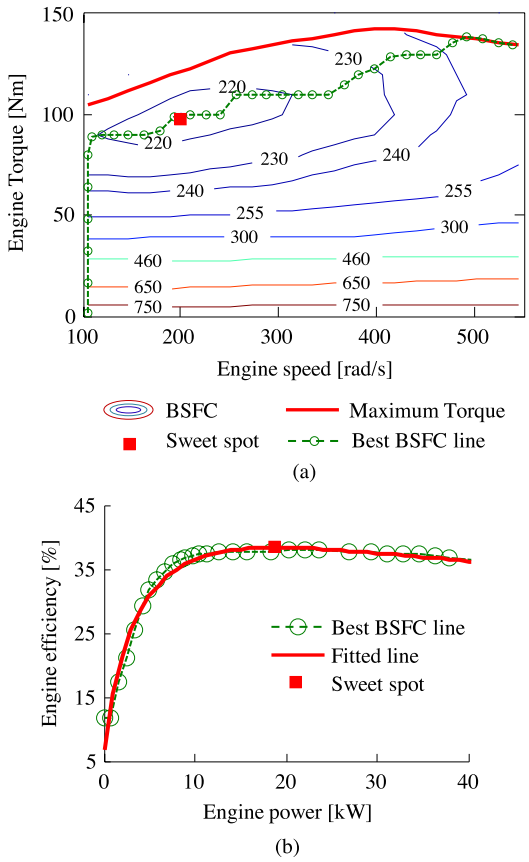

Fig. 2. Engine model. (a) BSFC map (in grams per kilowatt-hour). (b) Efficiency of the best BSFC line.

Note that all of the energy stored in the battery is derived from the engine, making the battery an energy buffer rather than an original source. To ensure charge sustenance, the initial and terminal states of the SOC are constrained to be the same in this fuel-optimal cruising problem.

B. Vehicle Dynamics for Control

In the parallel HEV, the engine and the motor can drive the vehicle together or separately. Based on the force balance equations, distance s and velocity v satisfy

$$\begin{aligned} \dot{s} &= v \\ \dot{v} &= \frac{\eta_C P_e + P_m - F_r(v)v}{Mv} \\ F_r(v) &= 0.5\, C_D \rho_a A_v v^2 + Mgf \end{aligned} \tag{4}$$

where η_C is the efficiency of the CVT, P_m is the motor power, F_r is the aerodynamic drag and rolling resistance, C_D is the aerodynamic drag coefficient, ρ_a is the air density, A_v is the frontal area of the vehicle, f is the rolling resistance coefficient, and M and g represent the vehicle mass and the gravity constant. If the engine is off, the clutch can be disengaged to avoid engine drag, that is, $P_e = 0$. The motor power P_m can be either negative or positive, corresponding to charge mode or discharge mode, respectively.

The speed ratio i_C of the CVT determines the ratio between the vehicle speed and the engine speed, i.e.,

$$i_C = \frac{w_e r_w}{i_0 v} \tag{5}$$

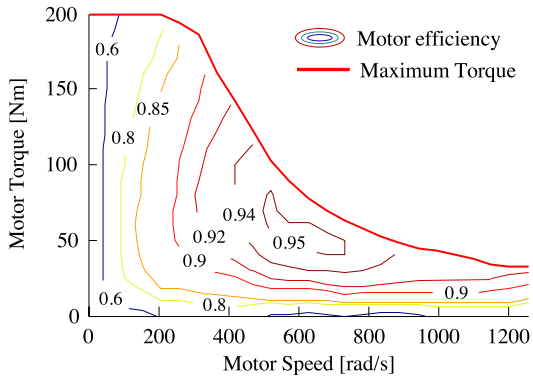

Fig. 3. Motor efficiency as a function of motor speed and torque.

where w_e is the engine speed, i_0 is the speed ratio of the final drive, and r_w is the tire radius. The mechanical efficiency of the CVT is nonlinear and depends on its speed ratio and load. For push-belt CVT, under high-speed ratio or high-power conditions, the efficiency is high (about 85%–90%); otherwise, it will rapidly deteriorate to about 70% [23], [24]. For hybrid vehicles, since the engine can eliminate low-power operations, the CVT can avoid inefficient operations. Under this assumption, the CVT efficiency is simplified as a η_C constant.

In addition to the given vehicle dynamics, the battery dynamics is expressed as [25]

$$\dot{SOC} = -\frac{V_{oc} - \sqrt{V_{oc}^2 - 4P_b \times R_{\text{int}}}}{2R_{\text{int}} \times C} \tag{6}$$

where SOC stands for the state of charge of the battery, V_{oc} is the battery voltage, R_{int} is the internal resistance, C is the battery capacity, and P_b is the battery power.

Battery power P_b relies on motor power P_m. In the charge mode, the motor acts as a generator and charges the battery. Both P_b and P_m are negative with the following relationship:

$$P_b = P_m \eta_m \quad P_m < 0. \tag{7}$$

In the discharge mode, P_b and P_m are both positive and governed by the following relationship:

$$P_b = \frac{P_m}{\eta_m} \quad P_m \geq 0 \tag{8}$$

where η_m is the efficiency of the motor, as shown in Fig. 3. It depends on motor speed w_m and torque T_m.

In this powertrain topology, motor speed w_m is related to the vehicle speed, i.e.,

$$w_m = \frac{i_m i_0 v}{r_w} \tag{9}$$

where i_m is the gear ratio of the torque coupler. Motor torque T_m is then obtained from

$$T_m = \frac{P_m}{w_m}. \tag{10}$$

We assume that the generator efficiency map is identical to the motor efficiency map, i.e.,

$$\eta_m(w_m, T_m) = \eta_m(w_m, -T_m). \tag{11}$$

C. Constraints for Inputs and States

Equality and inequality constraints arise from the physical limits of the engine, CVT, battery, and motor, including

$$\begin{aligned} P_{e,\min} \leq P_e \leq P_{e,\max} \\ i_{C,\min} \leq i_C \leq i_{C,\max} \\ \text{SOC}_{\min} \leq \text{SOC} \leq \text{SOC}_{\max} \\ T_{m,\min} \leq T_m \leq T_{m,\max} \\ w_{m,\min} \leq w_m \leq w_{m,\max}. \end{aligned} \tag{12}$$

In the cruising problem we are solving, initial velocity v_0 and terminal velocity v_f are set to be equal, i.e.,

$$v_0 = v_f. \tag{13}$$

Similarly, the initial and terminal states of the SOC are also forced to be the same, i.e.,

$$\text{SOC}_0 = \text{SOC}_f. \tag{14}$$

D. Optimal Control Problem

The resulting OCP is stated as follows:

$$\begin{aligned} \min \quad & J = \frac{\int_0^{t_f} \mathcal{F}_e dt}{s_f} \\ \text{subject to} \quad & \dot{s} = v \\ & \dot{v} = \frac{\eta_C P_e + P_m - F_r(v)v}{Mv} \\ & \dot{SOC} = -\frac{V_{oc} - \sqrt{V_{oc}^2 - 4P_b \times R_{\text{int}}}}{R_{\text{int}} \times C} \\ & P_b = \begin{cases} \frac{P_m}{\eta_m} & P_m \geq 0 \\ P_m \eta_m & P_m < 0 \end{cases} \\ & v_0 = v_f \\ & \text{SOC}_0 = \text{SOC}_f \\ & P_{e,\min} \leq P_e \leq P_{e,\max} \\ & i_{C,\min} \leq i_C \leq i_{C,\max} \\ & \text{SOC}_{\min} \leq \text{SOC} \leq \text{SOC}_{\max} \\ & T_{m,\min} \leq T_m \leq T_{m,\max} \\ & w_{m,\min} \leq w_m \leq w_{m,\max}. \end{aligned} \tag{15}$$

The states are distance s, velocity v, and SOC, which are denoted as $\boldsymbol{x} = (s, v, \text{SOC})^T$. The control inputs include engine power P_e and motor power P_m, which are denoted as $\boldsymbol{u} = (P_e, P_m)^T$. Except for the engine model and the motor model introduced in Section II-A and B, the other parameters are listed in Table I.

TABLE I
KEY PARAMETERS OF THE VEHICLE DYNAMICS

Parameters	Value	Parameters	Value
M	1450 kg	η_0	-10.06
C_D	0.28	P_0	3 kW
A_v	2.52 m^2	$P_{e,\max}$	60 kW
ρ_a	1.2 kg/m^3	$P_{e,\min}$	0
f	0.015	$i_{C,\max}$	0.4
r_w	0.287 m	$i_{C,\min}$	4.2
i_0	3.3	$w_{m,\max}$	1200 rad/s
i_m	2.63	$w_{m,\min}$	0
η_C	0.88	$SOC_{\max}$	80%
C	1.35 kWh	$SOC_{\min}$	30%
k_0, k_1, k_2	0.0253, -2.94922, 8.0482		

This OCP with strong nonlinearity in dynamics and discontinuity in switching between charge/discharge modes is challenging to solve. To address this discontinuous nonlinear problem, we employ the Legendre pseudospectral method (LPM) and the knotting technique to convert the OCP into a nonlinear programming (NLP) problem for more accurate numerical computation.

III. LEGENDRE PSEUDOSPECTRAL METHOD AND KNOTTING TECHNIQUE

The LPM is a global collocation method for converting OCP into NLP [26]–[28]. To convert the OCP into an associated NLP, it discretizes the OCP at orthogonal collocation points and then employs global interpolating polynomials to approximate states and control inputs. Compared with conventional methods (e.g., shooting method), the LPM has better accuracy and convergence speed [26]. It should be noted that the LPM is highly accurate only for smooth problems, thus unable to handle the nonsmooth OCP (15), which involves switching between different modes, namely, charge and discharge [27]. Here, we first simplify the switching rule and then apply the knotting technique to convert the OCP [27].

Since the initial and terminal states of the SOC must be the same, there are two possible cases: 1) Both the engine and the battery are used with no net change in battery energy, or 2) only the engine is used, which is a special case of 1) with the battery power always equal to zero. In the long run, there may be many charge/discharge events, whose optimal profile is difficult to obtain by this strong nonlinear and nonconvex OCP. Therefore, here, we focus on only one charge/discharge event over a shorter period of time. Under this simplification, the knotting technique is then utilized to convert the nonsmooth problem. Its fundamental idea is to divide the original OCP into two smooth substages, corresponding to the charge and discharge modes, and then, each of them is converted into an NLP by the LPM. To ensure continuity of the states (e.g., vehicle speed and SOC), connection constraints are added between the consecutive stages and, thus, relink the two local trajectories into an integrated continuous trajectory. The optimal results are eventually obtained by the collaborative optimization of the two substages. This technique can avoid accuracy loss compared with using only one smoothing function to approximate a nonsmooth trajectory. The process of converting the OCP by the LPM and the knotting technique is stated as follows. To be concise, the initial time is denoted as T_0, and the terminal time of the two substages is denoted as T_1 and T_2.

a) Conversion of Time Interval: The two stages are transformed into a canonical interval $[-1, 1]$ by

$$\tau = \frac{2t - (T_q + T_{q-1})}{T_q - T_{q-1}} \tag{16}$$

where q is 1 or 2.

b) Collocation Points and Approximation: The LPM employs Legendre–Gauss–Lobatto collocation points, which are the roots of the derivative of an Nth-order Legendre polynomial, together with two end points: -1 and 1. Each phase can have a different number of collocation points, which is denoted as $N_q + 1$. The collocation points at the qth phase are denoted as $\tau_{q,i}$, where $i = 0, 1, \ldots, N_q$. The states s, v, and SOC are discretized to

$$\boldsymbol{X}_q = \begin{bmatrix} \mathbb{S}_{q,0} & \mathbb{S}_{q,1} & \cdots & \mathbb{S}_{q,Nq} \\ \mathbb{V}_{q,0} & \mathbb{V}_{q,1} & \cdots & \mathbb{V}_{q,Nq} \\ \mathcal{S}_{q,0} & \mathcal{S}_{q,1} & \cdots & \mathcal{S}_{q,Nq} \end{bmatrix}. \tag{17}$$

Engine power P_e and motor power P_m are also discretized to $\mathbb{P}_{eq,i}$ and $\mathbb{P}_{mq,i}$. Note that we only optimize the discretized states and control inputs; the dynamic $\boldsymbol{x}_q(\tau)$ and $\boldsymbol{u}_q(\tau)$ are obtained by Lagrange interpolation at collocations points, i.e.,

$$\begin{aligned} \boldsymbol{x}_q(\tau) &\approx \sum_{i=0}^{Nq} L_{q,i}(\tau) \boldsymbol{X}_{q,i} \\ \boldsymbol{u}_q(\tau) &\approx \sum_{i=0}^{Nq} L_{q,i}(\tau) \boldsymbol{U}_{q,i} \end{aligned} \tag{18}$$

where $L_{q,i}(\tau)$ are the Lagrange basis polynomials.

c) Conversion of the State-Space Equations: The differential state equations can be approximated by the differential operation on the Lagrange basis polynomials, i.e.,

$$\dot{\boldsymbol{x}}_q(\tau_{q,k}) = \sum_{i=0}^{Nq} \dot{L}_{q,i}(\tau_{q,k}) \boldsymbol{X}_{q,i} = \sum_{i=0}^{Nq} D_{ki}^q \boldsymbol{X}_{q,i} \tag{19}$$

where $k = 0, 1, 2, \ldots, N_q$, and $\boldsymbol{D}^q$ is the differentiation matrix with an explicit expression [26]. Then, the vehicle dynamics (4) and battery dynamics (6) are converted into a series of equality constraints at the collocation points, i.e.,

$$\begin{aligned} &\sum_{i=0}^{N_q} D_{ki}^q \mathbb{S}_{q,i} = \Delta T_q \times \mathbb{V}_{q,k} \\ &\sum_{i=0}^{N_q} D_{ki}^q \mathbb{V}_{q,i} = \Delta T_q \frac{\eta_C \mathbb{P}_{eq,k} + \mathbb{P}_{mq,k} - F_r(\mathbb{V}_{q,k}) \mathbb{V}_{q,k}}{M \mathbb{V}_{q,k}} \\ &\sum_{i=0}^{N_q} D_{ki}^q \mathcal{S}_{q,i} = -\Delta T_q \frac{V_{oc} - \sqrt{V_{oc}^2 - 4 \mathbb{P}_{bq,k} \times R_{\text{int}}}}{2 R_{\text{int}} \times C} \end{aligned} \tag{20}$$

where $\Delta T_q = (T_q - T_{q-1})/2$.

d) Conversion of the Cost Function: The integral part of the cost function is calculated by the Gaussian–Lobatto quadrature; hence, the performance index is computed by

$$J=\sum_{q=1}^{2}\frac{\Delta T_q\sum_{k=0}^{N_q}w_{q,k}\mathcal{F}_e(\mathbb{P}_{eq,k})}{\mathbb{S}_{2,N_2}} \tag{21}$$

where $w_{q,k}$ are the weighting coefficients of the Gaussian–Lobatto quadrature, which is defined as [26]

$$w_{q,k}=\int_{-1}^{1}L_{q,k}(\tau)d\tau=\frac{2}{N_q(N_q+1)P_{N_q}^2(\tau_{q,k})}. \tag{22}$$

e) Connection Constraints: Since the distance, velocity, and SOC are continuous between the two stages, the following constraints are added:

$$\begin{aligned}\mathbb{S}_{1,N_1}-\mathbb{S}_{2,0}&=0\\ \mathbb{V}_{1,N_1}-\mathbb{V}_{2,0}&=0\\ \mathcal{S}_{1,N_1}-\mathcal{S}_{2,0}&=0.\end{aligned} \tag{23}$$

After these steps, the OCP (15) is converted into the following NLP problem:

$$J=\sum_{q=1}^{2}\frac{\Delta T_q\sum_{k=0}^{N_q}w_{q,k}\mathcal{F}_e(\mathbb{P}_{eq,k})}{\mathbb{S}_{2,N_2}}$$

subject to

$$\begin{aligned}&\sum_{i=0}^{N_q}D_{ki}^q\mathbb{S}_{q,i}=\Delta T_q\times\mathbb{V}_{q,k}\\ &\sum_{i=0}^{N_q}D_{ki}^q\mathbb{V}_{q,i}=\Delta T_q\frac{\eta_C\mathbb{P}_{eq,k}+\mathbb{P}_{mq,k}-F_r(\mathbb{V}_{q,k})\mathbb{V}_{q,k}}{M\mathbb{V}_{q,k}}\\ &\sum_{i=0}^{N_q}D_{ki}^q\mathcal{S}_{q,i}=-\Delta T_q\frac{V_{oc}-\sqrt{V_{oc}^2-4\mathbb{P}_{bq,k}\times R_{\rm int}}}{2R_{\rm int}\times C}\\ &\mathbb{P}_{bq,k}=\begin{cases}\dfrac{\mathbb{P}_{mq,k}}{\eta_m}, & \mathbb{P}_{mq,k}\geq 0\\ \mathbb{P}_{mq,k}\eta_m, & \mathbb{P}_{mq,k}<0\end{cases}\\ &\mathbb{V}_{1,0}=\mathbb{V}_{2,N_2}\\ &\mathcal{S}_{1,0}=\mathcal{S}_{2,N_2}\\ &\mathbb{S}_{1,N_1}=\mathbb{S}_{2,0}\\ &\mathbb{V}_{1,N_1}=\mathbb{V}_{2,0}\\ &\mathcal{S}_{1,N_1}=\mathcal{S}_{2,0}\\ &P_{e,\min}\leq\mathbb{P}_{eq,k}\leq P_{e,\max}\\ &i_{C,\min}\leq i_C\leq i_{C,\max}\end{aligned} \tag{24}$$

where $k,i=0,1,2,\ldots,N_q;q=1,2$. The variables to be optimized include traveling distance $\mathbb{S}_{q,k}$, vehicle speed $\mathbb{V}_{q,k}$, SOC of battery $\mathcal{S}_{q,k}$, engine power $\mathbb{P}_{eq,k}$, and motor power $\mathbb{P}_{mq,k}$. In essence, this NLP is a high-dimensional sparse-constrained problem and is solved by the sequential quadratic programming algorithm [29].

IV. Optimization Results

This section presents the fuel-optimal cruising strategies, including their fuel-saving performance and the control rules for the engine and the motor.

A. Speed-PnG Cruising Operation

Considering that the vehicle is expected to cruise at a certain average speed, we first focus on the general case, in which the vehicle speed is free. In this case, the average speed $\bar{v}$ must be equal to the expected speed v_e, i.e.,

$$\bar{v}=\frac{s_f}{t_f}=v_e. \tag{25}$$

The initial/final SOCs are set to 50%. The terminal time is fixed to 20 s. The number of collocation points in each phase is set to 15. Three cases, cruising at $v_e=20$, 60, and 120 km/h, are studied. By using the LPM and the knotting technique, their optimal profiles of speed fluctuation, SOC, and engine power are obtained and shown in Fig. 4. Then, we make the following observations.

1) In the cases of 20 and 60 km/h, the fuel-optimal operation accelerates the vehicle to a higher speed first and then coasts down to a lower speed, as shown in Fig. 4(a). The speed fluctuations of the two cases are $\pm 26\%$ and $\pm 9\%$, respectively. In Fig. 4(b), the SOC is constant for the whole duration of the two cases, which means that no energy is converted to the battery, and the battery/motor systems are not used. In Fig. 4(c), the engine first runs at high power, which approximately coincides with the power of the sweet spot, and then switches to shutdown with zero-power output.

   Due to the fixed SOC and fluctuating speed, that is, the vehicle speed ***pulses*** first and then ***glides***, this optimal strategy is called "Speed-PnG" operation, consisting of the pulse phase and the glide phase.

   This optimal strategy shows that 1) counter to the intuition that cruising at a fixed speed is fuel optimal, the true optimum is Speed-PnG operation; 2) when cruising at low speeds (e.g., 20 km/h), the battery and the motor are not used, and the optimal control rule for the engine is to switch between the sweet spot and shut down, corresponding to the pulse/glide phases.
2) In the case of 120 km/h, the vehicle speed, SOC, and engine power are all constant. The optimal operation is cruising at a fixed speed driven by the engine only. This optimal strategy is called "CS" (constant speed) operation.

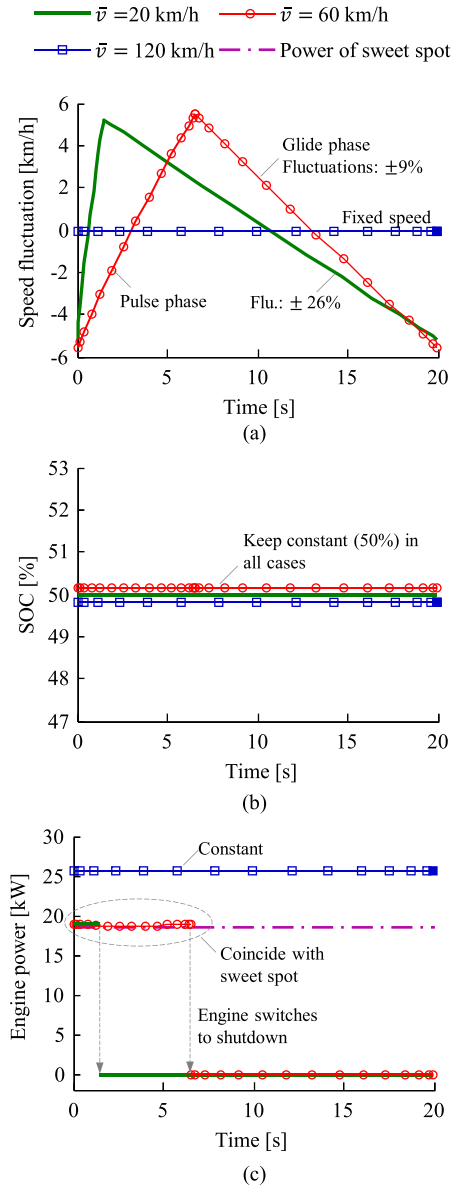

Fig. 4. Optimization results. Speed-PnG strategy at 20 and 60 km/h and CS strategy at 120 km/h. (a) Speed profile. (b) SOC. (c) Engine power.

To understand the fuel economy of Speed-PnG, we set the CS operation as the benchmark. In the cases of 20 and 60 km/h, the fuel consumption of using CS is 4.30 and 3.47 L/100 km, respectively, dropping to 2.03 and 2.97 L/100 km if using Speed-PnG. Therefore, Speed-PnG achieves a fuel savings of 52.7% and 14.45% compared with CS, with a fuel-saving rate ($\eta_{\mathcal{F}}$) defined as

$$\eta_{\mathcal{F}} = \frac{J_{\mathrm{CS}} - J_{\mathrm{PnG}}}{J_{\mathrm{CS}}} \times 100\% \tag{26}$$

where J_{CS} and J_{PnG} are fuel consumed by CS and PnG.

With expanding the three given examples to various average cruising speeds, the fuel-saving rate of Speed-PnG and the corresponding average optimal engine power to pulse are shown in Fig. 5. When $\bar{v} \in [20, 104]$ km/h, the Speed-PnG strategy achieves better fuel economy than CS, and the optimal operating engine power is approximately equal to the power of the sweet spot.

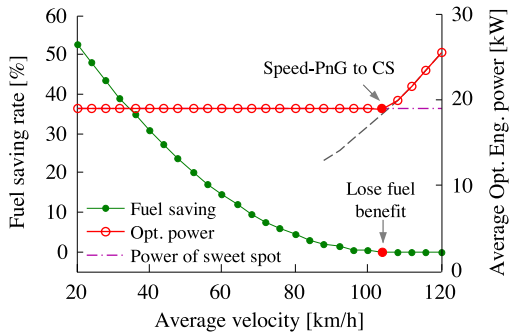

Fig. 5. Optimal fuel-saving rate and average engine power in the pulse phase of Speed-PnG at different average cruising speeds.

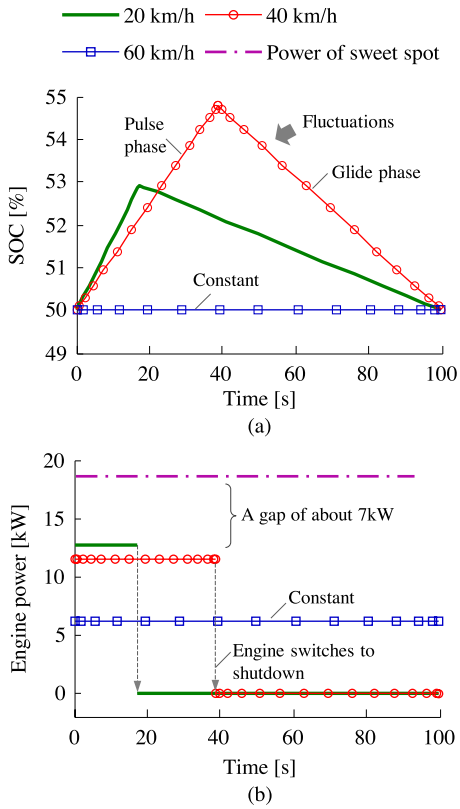

Fig. 6. Optimization results. SOC-PnG strategy at 20 and 40 km/h and CS strategy at 60 km/h. (a) SOC profile. (b) Engine power.

B. SOC-PnG Cruising Operation

In the Speed-PnG operation, the fluctuating speed is less acceptable for human drivers. Hence, here, we tighten the constraint on vehicle speed to cruising at a fixed speed rather than pulse and glide, i.e.,

$$v \equiv v_e. \tag{27}$$

The terminal time is set to 100 s, and the initial/final SOCs are set to 50%. Three cases, i.e., cruising at 20, 40, and 60 km/h, are selected, and the optimization results are shown in Fig. 6, which shows the following observations.

1) In the cases of 20 and 40 km/h, the engine first operates at high power to maintain vehicle cruising and charge the battery, with the SOC rising; then, the engine is shut

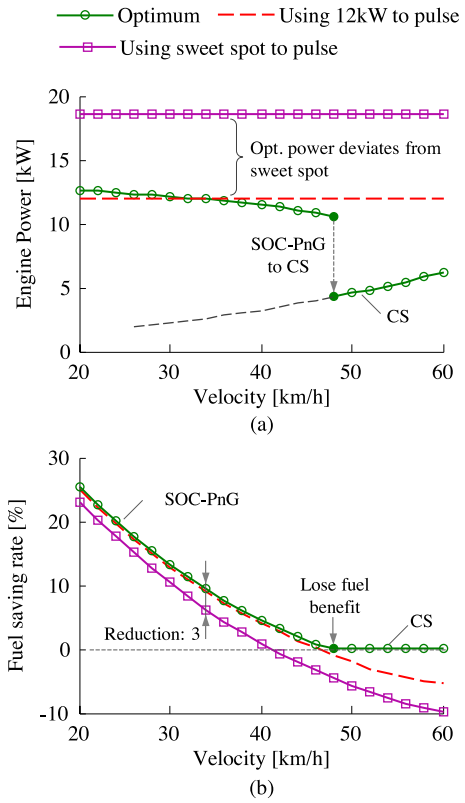

Fig. 7. Optimal average engine power and fuel-saving rate of SOC-PnG at different cruising speeds. (a) Optimal engine power. (b) Fuel savings compared with the CS strategy.

down, and only the battery is used to drive the vehicle, with the SOC dropping to the initial value.

Due to the fluctuating SOC, where the SOC ***pulses*** first and then ***glides***, this strategy is called "SOC-PnG" operation. Fig. 6(b) shows that the optimal engine power in the pulse phase is 12.65 and 11.44 kW at 20 and 40 km/h, respectively. They differ from the power of the sweet spot (18.9 kW), which is generally considered to be optimal. This result will be explained in the following section.

2) When cruising at 60 km/h, the SOC is constant (50%), and the engine keeps operating at 6.13 kW, indicating that the vehicle is driven by the engine only. Therefore, the optimal operation is CS rather than SOC-PnG.

In the first two cases, the fuel consumption using the SOC-PnG strategies is 3.22 and 3.30 L/100 km, rising to 4.30 and 3.45 L/100 km if using CS, respectively. Thus, SOC-PnG achieves fuel savings of 25.1% and 4.3% compared with CS. With individually optimizing the problems at different cruising speeds, the fuel-saving rate and optimal engine power to pulse are shown in Fig. 7. When $v \leq 48$ km/h, SOC-PnG can save fuel, and its optimal engine power is around 12 kW. As the cruising speed increases, the fuel-saving rate continuously decreases, and, eventually, CS becomes optimal. The mechanism of the given results is discussed in Section V.

To understand the optimal engine power deviating from the sweet spot in Fig. 7(a), the case of keeping the engine operating at the sweet spot (18.9 kW) to pulse is simulated in Fig. 7(b).

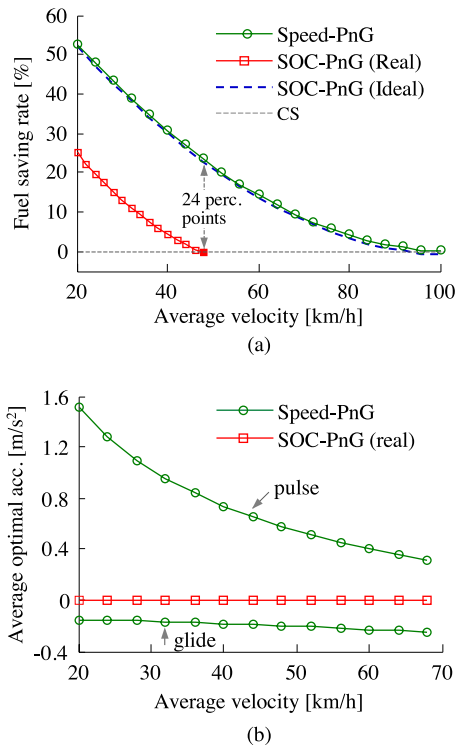

Fig. 8. Comparison of Speed-PnG and SOC-PnG (real/ideal). (a) Fuel-saving rate. (b) Average optimal acceleration.

It indicates that the fuel-saving rate drops about 3% compared with the SOC-PnG at optimum. As a simplification, keeping the engine running at fixed 12 kW only leads to less than 1% reduction. Overall, in the SOC-PnG operation, selecting a proper lower engine power to pulse can achieve better fuel performance than using the sweet spot.

C. Comparison Between Speed-PnG and SOC-PnG

As mentioned in the given optimizations, both Speed-PnG and SOC-PnG can save fuel compared with CS in a particular speed interval. Their optimal fuel-saving rates are shown in Fig. 8(a), where the Speed-PnG strategy has better fuel economy than SOC-PnG. As the average speed increases, the fuel-saving capacity of both operations decreases and eventually vanishes.

For the SOC-PnG strategy, if the battery and the motor are ideal (with 100% efficiency), which is denoted as SOC-PnG (ideal), then we can operate the engine at the sweet spot to charge the battery, without conversion loss. Theoretically, it has the highest system efficiency. In Fig. 8(a), the Speed-PnG strategy achieves similar fuel economy with SOC-PnG (ideal), indicating that Speed-PnG is the most efficient mode of operation.

Considering ride comfort, however, the Speed-PnG strategy is less acceptable due to the fluctuating speed. The average optimal accelerations of Speed-PnG and SOC-PnG at various average cruising speeds are shown in Fig. 8(b). In practice, a tradeoff between fuel economy and ride comfort is possible; the compromise principles are proposed in Section VI.

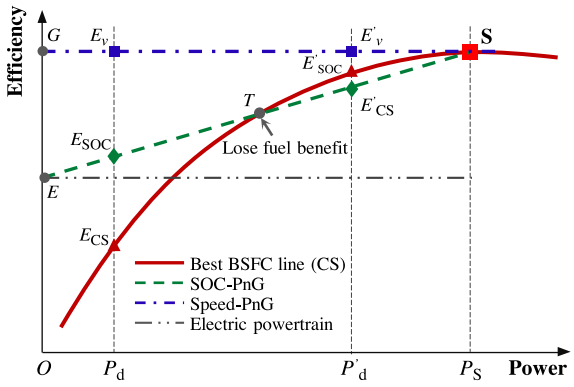

Fig. 9. Mechanism of Speed-PnG and SOC-PnG.

V. Fuel-Saving Mechanisms

Here, we focus on explaining the underlying mechanisms of Speed-PnG and SOC-PnG by addressing the following questions:

- Q1) Why does Speed-PnG save fuel at a certain speed interval, and why is it the most efficient operation?
- Q2) Why can SOC-PnG save fuel, and why is its fuel-saving capacity lower than that of Speed-PnG?
- Q3) In Speed-PnG, why does the optimal control operate the engine between the sweet spot and shut down without using the battery/motor system?
- Q4) In SOC-PnG, why does the engine not operate at the sweet spot to minimize fuel consumption?

Fig. 9 is designed as the key figure for understanding the mechanisms and answering the questions. The abscissa is power; the ordinate is efficiency. If the vehicle cruises at a fixed speed v, the demanded engine power is recorded as P_d. Since the engine always operates on the best BSFC line, point $E_{\rm CS}$ stands for the corresponding engine efficiency of using the CS strategy.

For Q1, in Speed-PnG, the engine operates at the sweet spot S with highest efficiency η_S in the pulse phase. In the glide phase, the engine is shut down, and the vehicle coasts, dissipating the stored kinetic energy, which is generated in the pulse phase with efficiency η_S. Therefore, points S/G stand for the pulse/glide phases, respectively. Ignoring the tiny difference of total aerodynamic drag in Speed-PnG and CS, the average engine power of Speed-PnG is equal to P_d; hence, point E_v indicates the average efficiency of Speed-PnG.

It is clear that the average efficiency (point E_v) of Speed-PnG is higher than that of CS (point $E_{\rm CS}$). As the average cruising speed increases (e.g., point P_d moves to P'_d), the efficiency of Speed-PnG (point E'_v) remains fixed, whereas the efficiency of CS (point $E'_{\rm CS}$) increases. As a consequence, the fuel-saving rate decreases. When point P_d moves to P_S, the two strategies have the same efficiency, at which point, Speed-PnG loses its fuel benefit, and CS becomes the optimal operation.

In Speed-PnG, the vehicle body actually plays the role of an energy buffer with variable kinetic energy, and the kinetic energy can be "charged/discharged" with 100% efficiency, thus making Speed-PnG the most efficient operation.

For Q2, to be concise, here, we assume the following.

a) The motor efficiency η_m and the discharge/charge efficiency $\eta_{\rm dis}/\eta_{\rm chg}$ of the battery are fixed.
b) In the pulse phase, the engine operates at sweet spot S to charge the battery and drive the vehicle, although it is not the optimum, as shown in Fig. 7.

In the glide phase, the engine is shut down, and the motor drives the vehicle using the stored energy in the pulse phase. The motor-output energy originates from the engine with the following conversion steps: engine $(\eta_S) \rightarrow$ motor $(\eta_m) \rightarrow (\eta_{\rm chg})$ battery $(\eta_{\rm dis}) \rightarrow$ motor $(\eta_m) \rightarrow$ vehicle, where $\eta_\#$ is the efficiency. The overall efficiency is recorded as $\eta_E = \eta_S\eta_m\eta_{\rm chg}\eta_{\rm dis}\eta_m$. It is called the efficiency of electric powertrain, as shown in Fig. 9.

Here, we argue that the efficiency of SOC-PnG is on line ES; the proof is given as follows.

Record the duration of the pulse phase as T_p, the total fuel consumption $\mathcal{F}_c$ is

$$\mathcal{F}_c = \frac{t_P P_S}{c_g \eta_S} \tag{28}$$

where c_g is the calorific value of gasoline. Energy E_b charged to the battery is

$$E_b = t_P(P_S - P_d)\eta_m\eta_{\rm chg}. \tag{29}$$

In the glide phase, the stored energy is consumed, and the duration t_G is

$$t_G = \frac{E_b\eta_{\rm dis}\eta_m}{P_d}. \tag{30}$$

Thus, the average efficiency $\eta_{\rm SOC}$ of SOC-PnG is

$$\begin{aligned}\eta_{\rm SOC} &= \frac{P_d(t_p + t_G)}{c_g\mathcal{F}_c} \\ &= \eta_E + \frac{P_d}{P_S}(\eta_S - \eta_E).\end{aligned} \tag{31}$$

This formula shows that $\eta_{\rm SOC}$ is a linear function of P_d, with $\eta_{\rm SOC} = \eta_E$ when $P_d = 0$ and $\eta_{\rm SOC} = \eta_S$ when $P_d = P_S$. Point $E_{\rm SOC}$ thus stands for the average efficiency of SOC-PnG when the demanded power is P_d.

In Fig. 9, point $E_{\rm SOC}$ is higher than point $E_{\rm CS}$ at low speed, allowing SOC-PnG to save fuel when $\bar{v} \leq 48$ km/h, as shown in Fig. 7. As the demanded power increases, point $E_{\rm SOC}$ linearly rises, and point $E_{\rm CS}$ nonlinearly increases. At point T, the two strategies have the same efficiency, at which point the optimal strategy changes from SOC-PnG to CS.

In SOC-PnG, the battery acts as the energy buffer to adjust the engine status. Compared with the vehicle body, the battery suffers about 10% conversion loss, along with the motor. Thus, SOC-PnG has lower fuel economy than Speed-PnG. If the battery/motor system is ideal with 100% efficiency, point E coincides with G, and then, point $E_{\rm SOC}$ coincides with E_v, which explains the similar fuel economy of SOC-PnG (ideal) and Speed-PnG (see Fig. 8).

For Q3, in Speed-PnG, letting the engine switch only between the sweet spot and shutdown, we can then obtain the highest average efficiency (line GS) and best fuel economy. To avoid the conversion loss of the battery/motor system, the extra energy generated in the pulse phase is preferentially transferred to the vehicle body; thus, the battery/motor is not used.

For Q4, if the engine operates at a random point with power P and efficiency η, (31) can be varied as

$$\max_P \ \eta_{\text{SOC}} = \eta(P) \times \left(\beta_1 + \beta_2 \frac{P_d}{P}\right) \tag{32}$$

where $\beta_1 = \eta_{\text{chg}}\eta_m\eta_{\text{dis}}\eta_m$ and $\beta_2 = 1 - \beta_1$ are constants. Operating the engine at point S maximizes the engine efficiency $\eta(P)$ but makes the last term $1/P$ deviate from the optimal. We can further convert (32) into (33), i.e.,

$$\max_P \ \eta_{\text{SOC}} = \eta(P) \times \left(1 - \beta_2 \frac{P - P_d}{P}\right) \tag{33}$$

where $\beta_2 = 1 - \eta_{\text{chg}}\eta_m\eta_{\text{dis}}\eta_m$ is the efficiency loss, and $P - P_d$ is the power converted into the battery. The last term reflects the conversion loss, and the higher P leads to greater loss. Therefore, the optimal engine power P is the tradeoff between engine efficiency and conversion loss. Note that for the real battery and motor, β_2 is related to P_d and P, and the optimal power (see Fig. 7) is determined by a more complex nonlinear optimization problem.

VI. Compromise Rules and Performance

Despite the highest fuel-saving rate, the Speed-PnG strategy suffers from poor ride comfort due to the fluctuating speed, as shown in Fig. 8. Here, we present the principles to compromise between fuel economy and ride comfort, that is, to limit the acceleration in the pulse phase by sacrificing fuel savings.

Based on Fig. 9, two rules are proposed to achieve the goal.

Rule A: In the pulse phase, for a given lower acceleration, the engine always operates at the sweet spot, but only part of the power is used to accelerate; the extra power is absorbed by the battery and later dissipated in the glide phase. In this case, both vehicle speed and SOC periodically fluctuate.

Rule B: In the pulse phase, for a given lower acceleration, the battery and motor are not used; the engine operates at lower power (lower efficiency) to accelerate rather than at the sweet spot (best efficiency), for example, using point T to replace the sweet spot S, as shown in Fig. 9.

The fuel-saving rate of Rule A and Rule B at different acceleration levels and average speed is shown in Fig. 10(a) and (b).

In Rule A, as the acceleration decreases, we can gain better ride comfort but lose more fuel benefit. Fig. 10(a) shows that the fuel-saving rate drops from the optimum (Speed-PnG) to that of SOC-PnG at a roughly linear rate. In effect, the lower the acceleration, the more power converted to the battery, thus leading to greater conversion loss. This compromise rule can be regarded as a weighted sum of Speed-PnG and SOC-PnG. Designers can determine the weights based on their relative demand for fuel economy and comfort.

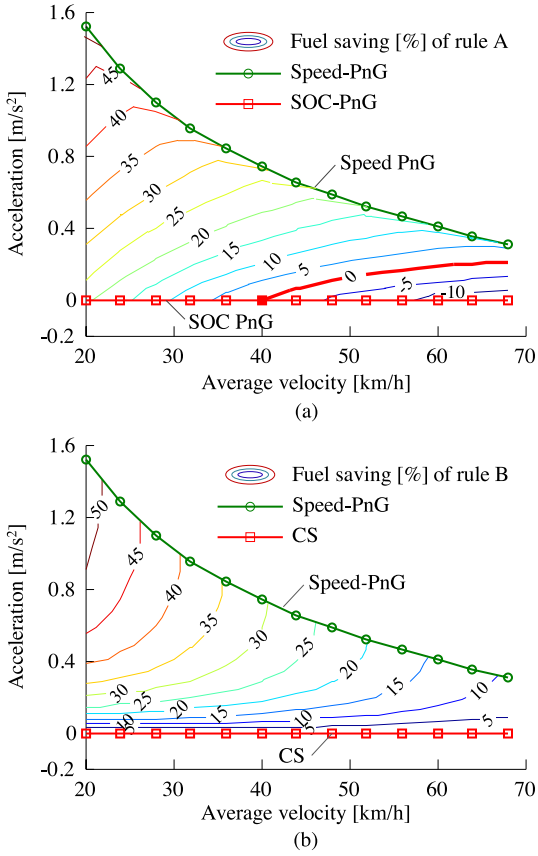

Fig. 10. Fuel economy of the two compromise strategies. (a) Fuel-saving map of Rule A. (b) Fuel-saving map of Rule B.

In Rule B, the fuel-saving rate drops from the optimum (Speed-PnG) to that of the CS strategy as the acceleration decreases. Due to the nonlinear engine efficiency, the fuel-saving rate drops slowly at first and then quickly descends to zero. It can be explained by Fig. 9: As point S moves left, line GS moves down, and then, point E_v goes down nonlinearly, depending on the profile of the best BSFC line. This rule can be regarded as a weighted sum of Speed-PnG and CS.

Fig. 11 shows the difference of Rule A and Rule B. Under high speed and high acceleration, Rule B achieves better fuel savings than Rule A. Otherwise, Rule A is more economical. In practice, drivers or control system can choose an acceptable acceleration level based on their preference for fuel economy or ride comfort and then determine the proper compromising control rule using Fig. 11.

VII. Conclusion

In this paper, we have studied the fuel-optimal cruising strategies for parallel HEVs. The main finding is that the battery/motor system and the inertia of the vehicle body could form a dual-energy-storage system. The vehicle inertia has higher energy conversion efficiency; its utilization can further improve the fuel efficiency but incur a penalty on ride comfort.

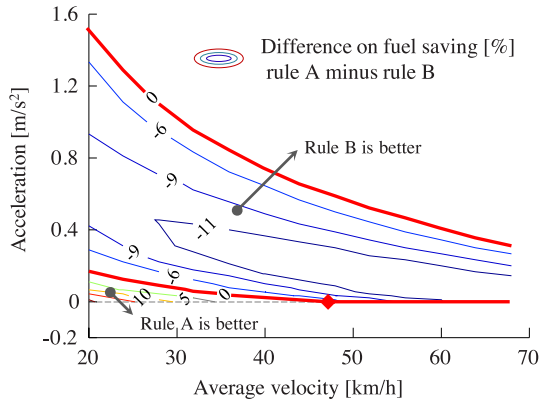

Fig. 11. Comparison of Rule A and Rule B (A minus B).

Therefore, their coordination enables better tradeoff between fuel economy and ride comfort. The detailed findings include the following.

1) Three fuel-optimal cruising strategies are proposed: Speed-PnG with fluctuating speed and fixed SOC, SOC-PnG with fluctuating SOC and fixed speed, and CS at a constant speed driven by the engine only.
   a) In free cruising scenarios with a limited average speed, the optimal operation is Speed-PnG at medium speed and then changes to CS at high speed. In Speed-PnG, the optimal control of the engine is to switch between the sweet spot and shutdown; the battery/motor system is not used to avoid conversion loss.
   b) In fixed-speed cruising scenarios, the optimal operation changes from SOC-PnG to CS at increasing speeds. In SOC-PnG, the engine does not operate at the sweet spot but at lower power (e.g., about 12 kW for the studied HEV), which is a tradeoff between engine efficiency and conversion loss.
2) Speed-PnG is the most efficient operation. It achieves better fuel economy than SOC-PnG, arising from the fact that vehicle inertia suffers from less conversion loss than the battery. Due to the two energy buffers, the engine can operate at an efficient region intermittently and avoid inefficient operation; thus, both Speed-PnG and SOC-PnG strategies have better fuel economy than the CS strategy.
3) In application, simultaneously using both vehicle inertia and battery can achieve better balance between fuel economy and ride comfort. For a limited acceleration, "decreasing the engine power without using the battery" is more efficient than "using the battery to absorb the extra energy with the engine operating at the sweet spot" under most conditions, except for the low-speed low-acceleration condition.

Generally, the Speed-PnG strategy with fluctuating kinetic energy could only be implemented in sparse traffic flow. To implement the proposed strategies, more issues such as coordinating with driver operation, executing in car-following scenarios, and its effect on the fuel economy and smoothness of the whole traffic flow should be further studied.

REFERENCES

[1] S. Clerides and T. Zachariadis, "The effect of standards and fuel prices on automobile fuel economy: An international analysis," *Energy Econ.*, vol. 30, no. 5, pp. 2657–2672, Sep. 2008.
[2] M. Kloess and A. Müller, "Simulating the impact of policy, energy prices and technological progress on the passenger car fleet in Austria—A model based analysis 2010–2050," *Energy Policy*, vol. 39, no. 9, pp. 5045–5062, Sep. 2011.
[3] H. H. Oliver, K. S. Gallagher, D. Tian, and J. Zhang, "China's fuel economy standards for passenger vehicles: Rationale, policy process, and impacts," *Energy Policy*, vol. 37, no. 11, pp. 4720–4729, Nov. 2009.
[4] R. D. Reitz, "Directions in internal combustion engine research," *Combustion Flame*, vol. 160, no. 1, pp. 1–8, Jan. 2013.
[5] K. A. N. G. Yong-Lin, "Lightweight vehicle, advanced high strength steel and energy-saving and emission reduction," *Iron Steel*, vol. 6, no. 2, pp. 1–12, 2008.
[6] G. Fontaras, P. Pistikopoulos, and Z. Samaras, "Experimental evaluation of hybrid vehicle fuel economy and pollutant emissions over real-world simulation driving cycles," *Atmos. Environ.*, vol. 42, no. 18, pp. 4023–4035, Jun. 2008.
[7] B. G. Pollet, I. Staffell, and J. L. Shang, "Current status of hybrid, battery and fuel cell electric vehicles: From electrochemistry to market prospects," *Electrochim. Acta*, vol. 84, pp. 235–249, Dec. 2012.
[8] A. Khaligh and Z. Li, "Battery, ultracapacitor, fuel cell, and hybrid energy storage systems for electric, hybrid electric, fuel cell, and plug-in hybrid electric vehicles: State of the art," *IEEE Trans. Veh. Technol.*, vol. 59, no. 6, pp. 2806–2814, Jul. 2010.
[9] D. Kum, H. Peng, and N. K. Bucknor, "Supervisory control of parallel hybrid electric vehicles for fuel and emission reduction," *J. Dyn. Syst., Meas., Control*, vol. 133, no. 6, 2011, Art. ID 061010.
[10] K. Ç Bayindir, M. A. Gözüküçük, and A. Teke, "A comprehensive overview of hybrid electric vehicle: Powertrain configurations, powertrain control techniques and electronic control units," *Energy Convers. Manage.*, vol. 52, no. 2, pp. 1305–1313, Feb. 2011.
[11] S. G. Wirasingha and A. Emadi, "Classification and review of control strategies for plug-in hybrid electric vehicles," *IEEE Trans. Veh. Technol.*, vol. 60, no. 1, pp. 111–122, Jan. 2011.
[12] H. Borhan *et al.*, "MPC-based energy management of a power-split hybrid electric vehicle," *IEEE Trans. Control Syst. Technol.*, vol. 20, no. 3, pp. 593–603, May 2012.
[13] K. Van Berkel, T. Hofman, B. Vroemen, and M. Steinbuch, "Optimal control of a mechanical hybrid powertrain," *IEEE Trans. Veh. Technol.*, vol. 61, no. 2, pp. 485–497, Feb. 2012.
[14] C. C. Chan, "The state of the art of electric, hybrid, and fuel cell vehicles," *Proc. IEEE*, vol. 95, no. 4, pp. 704–718, Apr. 2007.
[15] M. Duoba, H. Ng, and R. Larsen, "Characterization and comparison of two hybrid electric vehicles (HEVs)—Honda Insight and Toyota Prius," Soc. Automotive Eng. (SAE), Warrendale, PA, USA, Tech. Paper 2001-01-1335, 2001.
[16] H. Y. Tong, W. T. Hung, and C. S. Cheung, "On-road motor vehicle emissions and fuel consumption in urban driving conditions," *J. Air Waste Manage. Assoc.*, vol. 50, no. 4, pp. 543–554, 2000.
[17] A. Wang *et al.*, "On-road pollutant emission and fuel consumption characteristics of buses in Beijing," *J. Environ. Sci.*, vol. 23, no. 3, pp. 419–426, Mar. 2011.
[18] A. E. Atabani, I. A. Badruddin, S. Mekhilef, and A. S. Silitonga, "A review on global fuel economy standards, labels and technologies in the transportation sector," *Renew. Sustain. Energy Rev.*, vol. 15, no. 9, pp. 4586–4610, Dec. 2011.
[19] J. Lee, D. J. Nelson, and H. Lohse-Busch, "Vehicle inertia impact on fuel consumption of conventional and hybrid electric vehicles using acceleration and coast driving strategy," Soc. Automotive Eng. (SAE), Warrendale, PA, USA, Tech. Paper 2009-01-1322, 2009.
[20] S. E. Li and H. Peng, "Strategies to minimize the fuel consumption of passenger cars during car-following scenarios," *Proc. Inst. Mech. Eng., D, J. Automobile Eng.*, vol. 226, no. 3, pp. 419–429, Mar. 2012.
[21] S. E. Li, H. Peng, K. Li, and J. Wang, "Minimum fuel control strategy in automated car-following scenarios," *IEEE Trans. Veh. Technol.*, vol. 61, no. 3, pp. 998–1007, Mar. 2012.
[22] K. McDonough *et al.*, "Stochastic dynamic programming control policies for fuel efficient vehicle following," in *Proc. IEEE ACC*, Jun. 2013, pp. 1350–1355.
[23] M. A. Kluger and D. M. Long, "An overview of current automatic, manual and continuously variable transmission efficiencies and their projected future improvements," Soc. Automotive Eng. (SAE), Warrendale, PA, USA, Tech. Paper 1999-01-1259, 1999.

[24] T. Hofman, M. Steinbuch, R. van Druten, and A. F. Serrarens, "Design of CVT-based hybrid passenger cars," *IEEE Trans. Veh. Technol.*, vol. 58, no. 2, pp. 572–587, Feb. 2009.
[25] J. Liu and H. Peng, "Modeling and control of a power-split hybrid vehicle," *IEEE Trans. Control Syst. Technol.*, vol. 16, no. 6, pp. 1242–1251, Nov. 2008.
[26] G. Elnagar, M. A. Kazemi, and M. Razzaghi, "The pseudospectral Legendre method for discretizing optimal control problems," *IEEE Trans. Autom. Control*, vol. 40, no. 10, pp. 1793–1796, Oct. 1995.
[27] I. M. Ross and F. Fahroo, "Pseudospectral knotting methods for solving non-smooth optimal control problems," *J. Guid., Control, Dyn.*, vol. 27, no. 3, pp. 397–405, 2004.
[28] S. Xu, S. E. Li, K. Deng, S. Li, and B. Cheng, "A unified pseudospectral computational framework for optimal control of road vehicles," *IEEE/ASME Trans. Mechatron.*, vol. 20, no. 4, pp. 1–12, Aug. 2015.
[29] P. E. Gill, W. Murray, and M. A. Saunders, "SNOPT: An SQP algorithm for large-scale constrained optimization," *SIAM Rev.*, vol. 47, no. 1, pp. 99–131, 2005.

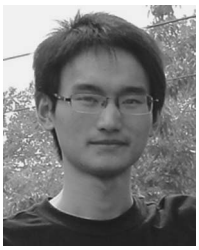

Shaobing Xu received the B.S. degree in automotive engineering from China Agricultural University, Beijing, China, in 2011. He is currently working toward the Ph.D. degree in automotive engineering with Tsinghua University, Beijing.

His research interests include optimal control theory and vehicle dynamics control.

Mr. Xu has received several awards and honors, including a National Scholarship, a President Scholarship, the first prize at the Chinese Fourth Mechanical-Design Contest, and the first prize in the 19th Advanced Mathematical Contest.

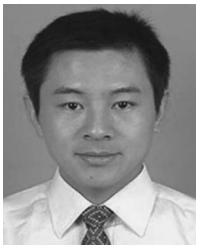

Shengbo Eben Li (M'11) received the M.S. and Ph.D. degrees in automotive engineering from Tsinghua University, Beijing, China, in 2006 and 2009, respectively.

In 2007, he was a Visiting Researcher with Stanford University, Stanford, CA, USA. From 2009 to 2011, he was a Postdoctoral Research Fellow with the University of Michigan, Ann Arbor, MI, USA. He is currently an Associate Professor with the Department of Automotive Engineering, Tsinghua University. His active research interests include autonomous vehicle control, optimal and predictive control, driver-assistance systems, and lithium-ion battery management.

Dr. Li received the Award for Science and Technology of China ITS Association in 2012, the Award for Technological Invention in Ministry of Education in 2012, the National Award for Technological Invention in China in 2013, and the Honored Funding for Beijing Excellent Youth Researcher in 2013.

Huei Peng received the Ph.D. degree in mechanical engineering from the University of California, Berkeley, CA, USA, in 1992.

He is currently a Professor with the Department of Mechanical Engineering, University of Michigan, Ann Arbor, MI, USA. His research interests include adaptive control and optimal control, with emphasis on their applications to vehicular and transportation systems. His current research focuses on the design and control of electrified vehicles and connected/automated vehicles.

Dr. Peng is a Fellow of the Society of Automotive Engineers and the American Society of Mechanical Engineers. He is a Changjiang Scholar with Tsinghua University, Beijing, China.

Bo Cheng received the B.S. and M.S. degrees in automotive engineering from Tsinghua University, Beijing, China, in 1985 and 1988, respectively, and the Ph.D. degree in mechanical engineering from Tokyo University, Tokyo, Japan, in 1998.

He is currently a Professor and the Dean of the Suzhou Automotive Research Institute with Tsinghua University. His active research interests include autonomous vehicles, driver-assistance systems, active safety, and vehicular ergonomics.

Dr. Cheng is the Chairman of the Academic Board of the Society of Automotive Engineers of China, a Member of the Council of the Chinese Ergonomics Society, and a Committee Member of the National 863 Plan.

Xiaowu Zhang received the B.S. degree from Beihang University, Beijing, China, in 2010 and the M.S. degree from the University of Michigan, Ann Arbor, MI, USA, in 2012, where he is currently working toward the Ph.D. degree, all in mechanical engineering.

His current research interests include optimal control, sizing and design of clean energy systems, and configuration design and control of split hybrid vehicles.

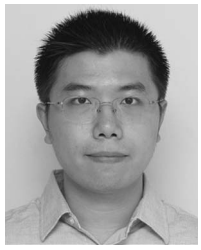

Ziheng Pan received the B.S. degree in automation from Sun Yat-sen University, Guangzhou, China, in 2010 and the M.S. degree in mechanical engineering from the University of Michigan, Ann Arbor, MI, USA, in 2012, where he is currently working toward the Ph.D. degree in mechanical engineering.

His current research interests include systematic design of multimode power-split hybrid vehicles and optimal design and control of vehicular propulsion systems.